

InfoPrint: Embedding Information into 3D Printed Objects

WEIWEI JIANG, The university of Melbourne, Australia

CHAOFAN WANG, The university of Melbourne, Australia

ZHANNA SARSENBAYEVA, The university of Melbourne, Australia

ANDREW IRLITTI, The university of Melbourne, Australia

JARROD KNIBBE, The university of Melbourne, Australia

TILMAN DINGLER, The university of Melbourne, Australia

JORGE GONCALVES, The university of Melbourne, Australia

VASSILIS KOSTAKOS, The university of Melbourne, Australia

We present a technique to embed information invisible to the eye inside 3D printed objects. The information is integrated in the object model, and then fabricated using off-the-shelf dual-head FDM (Fused Deposition Modeling) 3D printers. Our process does not require human intervention during or after printing with the integrated model. The information can be arbitrary symbols, such as icons, text, binary, or handwriting. To retrieve the information, we evaluate two different infrared-based imaging devices that are readily available – thermal cameras and near-infrared scanners. Based on our results, we propose design guidelines for a range of use cases to embed and extract hidden information. We demonstrate how our method can be used for different applications, such as interactive thermal displays, hidden board game tokens, tagging functional printed objects, and autographing non-fungible fabrication work.

Additional Key Words and Phrases: Digital fabrication, 3D print, information embedding, infrared imaging

1 INTRODUCTION

It is increasingly common to come across tagged objects in our daily life. The tags can be text, icons, barcodes or QR-codes printed or attached on an object’s surface. Using a tag is an effective way to enable object identification and augmentation. It can also help to link a physical object to a database with further information. This kind of augmentation is particularly helpful in providing design information for digitally fabricated objects, since they are often customized or personalized [16, 36].

Recent works show several promising ways to embed tags within digitally fabricated objects. Existing methods, however, have several issues. A common approach is to design a tag on the surface. This method can easily compromise the aesthetics of the object [36]. In comparison, the object design can be modified by extrusion or engraving for tagging [16]; however, this can also be obtrusive, and can limit the object’s functionality. Alternatively, recent work has shown promising results in embedding information under the surface, using high-end or professional 3D printers (e.g., PolyJet) [33, 77]. To date, however, such techniques have been unachievable with consumer-level FDM (Fused Deposition Modeling) printers, which are affordable, accessible and more suitable for many everyday use cases [58]. To

Authors’ addresses: Weiwei Jiang, weiwei.jiang@student.unimelb.edu.au, The university of Melbourne, Australia; Chaofan Wang, chaofanw@student.unimelb.edu.au, The university of Melbourne, Australia; Zhanna Sarsenbayeva, zhanna.sarsenbayeva@unimelb.edu.au, The university of Melbourne, Australia; Andrew Irlitti, andrew.irlitti@unimelb.edu.au, The university of Melbourne, Australia; Jarrod Knibbe, jarrod.knibbe@unimelb.edu.au, The university of Melbourne, Australia; Tilman Dingler, tilman.dingler@unimelb.edu.au, The university of Melbourne, Australia; Jorge Goncalves, jorge.goncalves@unimelb.edu.au, The university of Melbourne, Australia; Vassilis Kostakos, vassilis.kostakos@unimelb.edu.au, The university of Melbourne, Australia.

2021. Manuscript submitted to ACM

Manuscript submitted to ACM

1

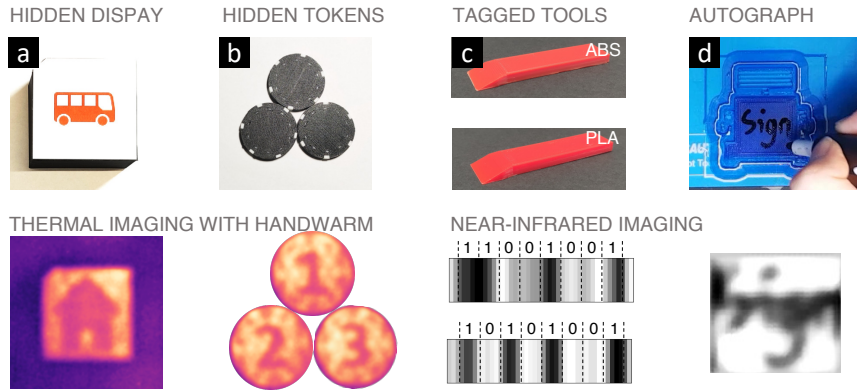


Fig. 1. Examples of *InfoPrint*: (a) A 3D printed hidden display with information both on and hidden under the surface. (b) Three identical models with hidden tags for social activities such as board games. (c) Two 3D printed tools using different materials with metadata (binary tags) under the top surfaces. The tags are durable with heavy use. (d) Autographing inside a 3D printed object. The autograph cannot be erased or modified as it is inside the object.

this end, we still lack an effective FDM 3D printer based tagging method that is printable with the object, and does not compromise its design aesthetics.

We present *InfoPrint*, a technique for invisibly embedding information (e.g., tags) into 3D printed objects using FDM 3D printers. The embedded information is unobtrusive or invisible to the eye. Our technique does not alter the surface design of the object, allowing for more creative and secure designs. With *InfoPrint*, it is possible to simply design and print information under the surface, without human intervention during or after printing.

To read the information, we leverage two methods for different use cases. One method is based on the different thermal conduction rate between the air and the 3D printed material. This is possible as most objects printed with an FDM 3D printer consist of an infill pattern with the majority of the space being filled with air. The information under the surface can be revealed using a thermal camera after applying heat to the surface (e.g., by hand-warming, as shown in Figure 1a and b). The second method is based on the fact that many plastic materials can be penetrated by or reflect near-infrared light [45]. By printing the information and the object using different materials or colors, the information can be read using a low-cost near-infrared device (Figure 1c and d).

Our contribution is three-fold. First, we present a technique to embed information into a 3D printed object using consumer-level FDM 3D printers. Our method expands the design space for tagging 3D printed objects without compromising their appearance or shape. Second, we provide comprehensive design guidelines for embedding information into 3D printed objects addressing multiple application scenarios and use cases. Third, we provide several example applications using an embedded information scheme, including a novel way to interact with digitally fabricated objects using thermal cameras, and a secure and non-fungible way to autograph a 3D printed object as a unique digital fabrication work.

2 RELATED WORK

2.1 Tagging 3D printed objects

2.1.1 Tagging on the surface.

An intuitive and convenient way to tag an object is to attach a label on the surface. For 3D printed objects, such a

label can also be printed as a part of the design or fabrication process [16]. For example, Harrison *et al.* proposed a notch pattern to tag a 3D printed object's surface. The notches can be swiped to generate a complex sound, which is then recorded by a microphone and decoded to a binary ID [21]. Similar work using a comb-like structure was presented by Savage *et al.* [49]. Besides acoustics, Maia *et al.* presented LayerCode, a scheme to embed optical barcodes by varying the colors of different layers, using a dual-color 3D printer [36]. However, LayerCode alters the appearance of the whole object, which can be undesirable. Although the authors demonstrated a method to make the information invisible, utilizing a customized material mixed with near-infrared dye and a modified 3D printer made the approach unrealistic for daily use. To address this issue, Delmotte [11] proposed a less restrictive method by varying the surface layer thickness. The authors developed a tool to manipulate the G-Code for tagging a 3D printed object on the surface. However, the area with the tag resembles printing flaws, and may be removed by daily use or during post-processing (e.g., polishing). This limitation also applies to the tagless method that utilizes subtle print artifacts or patterns for 3D printed object recognition [13].

In addition to binary tags mentioned above, existing works also show different ways to tag 3D printed objects with other textures. In particular, recent studies focus on incorporating textiles or fabrics in 3D objects to further expand the design space using FDM 3D printers with not only more applications, but also tagging methods by embedding textures on the printed objects. For instance, Rivera *et al.* demonstrated a technique to embed textiles into 3D printed objects, which can leverage well-developed embroidery techniques as a potential way for tagging [47]. Besides embedding, Takahashi *et al.* presented a method to print textiles using a 3D weaving technique [67]. The authors demonstrated that the fabrics can be printed using an FDM 3D printer by controlling the printer's head movements [67]. Alternatively, Forman *et al.* showed that such 3D printed quasi-fabrics could also be printed by under-extrusion [17]. Both works showed that 3D printed textiles with patterned textures can potentially be used as visual tags on the surface. It is worth noting that textile-like methods are mostly suitable for flexible objects, and may not be appropriate for long-term or heavy use.

Beyond visual patterns, researchers in the HCI community also developed methods to tag conductive patterns on the surface that can be read by a touchscreen. For example, Marky *et al.* showed a design to embed a conductive pattern on the bottom surface of an object. The pattern can be re-configured by the user, and thus, can be used for two-factor authentication in a tangible way [37]. Similarly, Schmitz *et al.* presented Itsy-Bits, a fabrication pipeline to design small footprints for detecting tangibles on a capacitive touchscreen [54]. However, their methods are limited to specific patterns and require user contact while reading, which may not be adopted to general information embedding applications.

Even though the use of 'on-the-surface' tagging methods is beneficial in several ways, such as convenience of labeling or intuition for reading, there are several important drawbacks. In particular, such a method can alter the appearance, shape or functionality of the object, and is less robust for long-term or frequent use.

2.1.2 Tagging under the surface.

In contrast to on-the-surface tagging methods, tagging an object under the surface is less intuitive or convenient to read. This method does not compromise the external design of the object, while also being more enduring. A common approach involves embedding an RFID tag inside a digitally fabricated object [63]. However, such a method requires additional materials and procedures to perform embedding, as a fully printable technique is not currently possible [15]. Our work addresses this issue and enables embedding information (*i.e.*, tagging) within a 3D printed object that is printable using an off-the-shelf FDM 3D printer.

A study by Li *et al.* is most closely related to our work [33]. The authors presented AirCode, a technique to embed a QR-Code like pattern under the surface of a 3D printed object. The code can be printed using a PolyJet 3D printer with well-designed cavities inside the 3D model. The code can then be read by a monochrome camera and a projector, and decoded as the tag of the printed object (*e.g.*, metadata or ID). However, AirCode cannot be used with the common consumer FDM 3D printer. This is because FDM 3D printers yield non-homogeneous printouts, and use relatively thick materials compared to an expensive PolyJet 3D printer. Also, AirCode only embeds binary data, and requires assembly after printing, since a PolyJet 3D printer cannot print hollows (cavities) inside an object. Another similar work is InfraStruts [77], an information embedding scheme for layered structures, allowing the embedding of not only binary data, but also icons and text. However, their method is also limited to PolyJet 3D printers and is susceptible to layer variations such as uniformed thickness, as the authors use a THz-TDS (TeraHertz Time-Domain) device for imaging. While there are prior examples of using FDM 3D printers to embed information, their design severely limits functionality in application and durability [60, 65]. Their methods are incapable of producing embedded information beyond binary due to their restrictive design between adjacent bits. Our approach does not have this limitation, and can produce binary, text and icons using a more accessible setting. Other works using highly customized materials make the settings unrealistic for daily use [59, 61, 62].

Beyond embedding information for imaging, recent works also include fabricating information as signals inside an object. For instance, Iyer *et al.* demonstrated a backscattering system that enables wireless analytics for 3D printed objects [28]. The authors embedded antennas that can be switched on or off using a sophisticated mechanical design, triggered by user interactions. The information can then be captured by reading the signals backscattered by the antennas. In another example, Chadalavada *et al.* presented ID'em [9] that allowed users to embed a conductive dot matrix under the surface that can be read by an array of inductive sensors. The conductive matrix works like an antenna array that manipulates the magnetic fields as the signals. The signals are then decoded as the information. However, both of the aforementioned methods are limited to specific data types (categorical or binary), and may not be easily printed using common off-the-shelf 3D printers.

2.2 Embedding objects with 3D prints

In a broad sense of information embedding, significant efforts have been done for embedding physical objects within 3D prints. In particular, researchers have focused on incorporating electronics with 3D printed objects that enable functionality or interactivity, *e.g.*, camera [48], a wireless accelerometer [24], or a speaker [27]. A recent study also demonstrated novel use cases enabling 3D printing on cloth with SMA (Shape-Memory Alloys) actuators [39]. Furthermore, researchers endeavor to provide tools and guidelines for designing inner structures to embed electronics, *e.g.*, for designing internal pipes [50, 76] or hollow tubes [68], optimizing sensor placement [6], component placement for assembly [12], or even for printed objects that are deformable [23, 32, 75] or re-configurable for fast-prototyping [55]. However, such methods are not fully printable yet, and cannot be automated. Therefore, it still requires relatively complex fabrication techniques with extra material costs, which is extravagant for simple tagging or information embedding tasks.

One way to overcome this non-printable disadvantage is to use the emerging conductive 3D printing materials. Recent works show potential to print conductive traces, circuits or surfaces within objects. For example, Schmitz *et al.* presented a design pipeline to print selected surfaces using conductive ABS (Acrylonitrile Butadiene Styrene) for sensing touched areas on a 3D printed object [52]. As an extension, the authors further showed a pipeline for embedding electrodes to fabricate a hover-, touch-, and force sensitive object [57]. Besides embedding electronics with the traces,

such a method can also be useful for various interactive scenarios in VR and AR [40]. Moreover, such a method can be adopted for heavily used functional objects utilizing emerging carbon fiber strengthened 3D print materials. For example, Swaminathan *et al.* demonstrated a technique to fabricate conductive traces while keeping the object mechanically strong for heavy use [66]. In addition to solid conductive traces, recent work has adopted conductive liquids for fabricating circuits using a 3D printed stamp as the circuit mold [69]. Beyond rigid objects, existing works also show the feasibility of embedding conductive traces or electronics for 3D printed flexible objects, such as conductive fabrics [43], electrospun textiles [46], using foldable structures [42, 78], or the flexible TPU (Thermoplastic Polyurethane) material with silver inks (*i.e.*, AgTPU) [70]. In particular for the flexible objects, researchers have strived to design a computational structure for enabling functionality or information embedding. For example, Schmitz *et al.* designed a flexible structure fabricated using TPU that can sense deformation as input information [56]. Deformation structures can also be used with pneumatic devices for sensing user inputs [22, 72]. Nevertheless, existing methods are not fully printable and still require electronics to be attached [35].

Beyond electronics, previous works also show other promising methods to embed everyday objects for 3D prints. In particular, Schmitz *et al.* demonstrated techniques to embed liquids inside 3D printed object as a changeable information, for sensing tasks such as tilting and motion [51, 53]. Such a method can also be beneficial for reducing cost of fabrication time or material, and has a great potential for information embedding [10, 38, 64, 74]. Other than 3D printing, researchers also proposed different digital fabrication based methods for information or object embedding, such as 3D sculpting [41], laser-cutting [67, 71], paper printing [34], or spraying [20].

In summary, existing works for embedding information inside a 3D printed object are not practical for general information embedding; they either require non-printable materials or cannot be applied to off-the-shelf consumer FDM 3D printers.

3 METHOD OVERVIEW

We present a technique to embed information under the surface of 3D printed objects. The embedded information itself is printable as part of the printed objects, and cannot be directly seen to the eye. In this section, we briefly describe the method to design, read, and fabricate.

3.1 Information embedding

Our design pipeline is shown in Figure 2. In this paper, we use Autodesk Fusion 360 [1] as the 3D modeling tool, without requiring any modification or plugin. Thus, the pipeline can also be applied to other 3D modeling software. The whole design pipeline includes three steps:

- (1) *Object modeling*: Model the desired object. For a mesh file (*e.g.*, stl file), Fusion 360 provides a “Mesh to BRep” function that allows readily editing the mesh file.
- (2) *Information modeling*: Model the necessary information (*e.g.*, letter ‘A’). The information should be sketched and extruded as a 3D object.
- (3) *Information Embedding*: Embed the information model inside the object model. Here, we embed the model for “A” into the object. Then the object model is subtracted by the “A” model, while keeping the “A” model in place. In Fusion 360, this can be achieved by invoking the “combine” command. For a mesh editor software, this can be achieved with “subtractive boolean” (*e.g.*, Blender [2]).

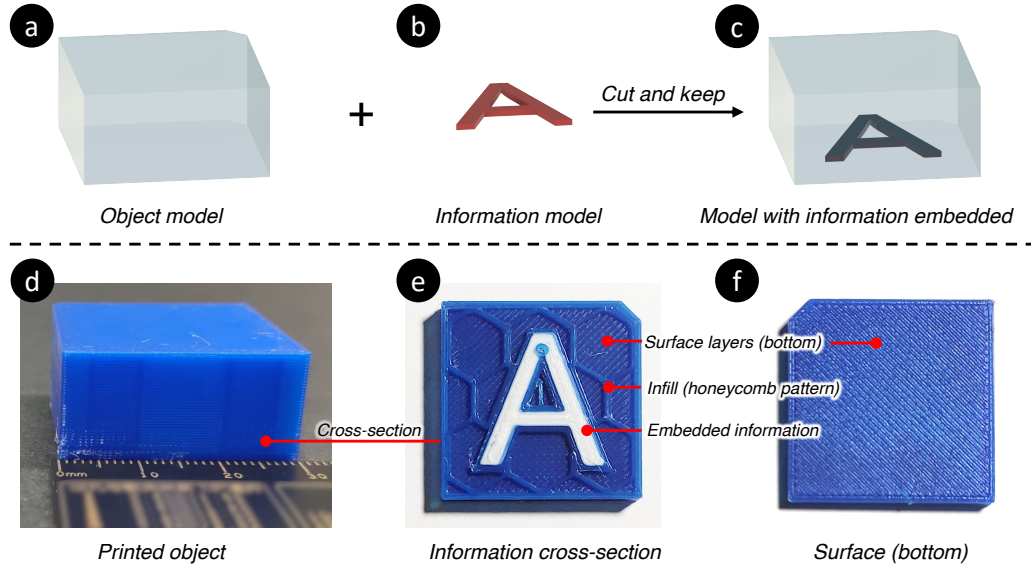


Fig. 2. Illustration of the design overview. (a) An object model to embed information inside. (b) The information model to be embedded. (c) The object model with information embedded. (d) The 3D printed object with information embedded. (e) The cross-section with information embedded. (f) The surface under which the information is embedded.

The designed model must be exported individually. In Fusion 360, the export option is “one file per body” for fabrication. This allows the slicing software to have different settings (such as materials) for the object model and the information model. For example, we demonstrate the fabricated object in Figure 2 (d)-(f), where the object is printed using PLA-Blue, while the information model is printed using PLA-White.

3.2 Reading principles

Since we aim to embed information that cannot be directly seen on the surface of the object, the information needs to be imaged (visualized) for reading. In this paper, we leverage the following two approaches for imaging:

- (1) *Thermal conduction*: As illustrated in Figure 3 (a), after heat is transferred to the surface of an object, the heat flows from that surface down into the object. Because the object’s inside is composed of two different materials, the heat permeates at different speeds, depending on thermal conduction properties of the materials. As a result, the temperature of the surface changes at different speeds, resulting in a thermal pattern as a projection of the information model on the surface. Here, we consider the filament materials (e.g., PLA or ABS) as one such material, while air is the other material (the spaces without infill).
- (2) *Light penetration and reflection*: As illustrated in Figure 3 (b), a 3D printed object can also be fabricated by two materials with different optical characteristics. In particular, we are interested in the case where the material on the surface layers can be penetrated while the other material inside the object is reflective. By transmitting light onto the surface of the object and measuring the reflected light, we can create an image of the reflection pattern. Further, as we aim to embed information unobtrusively, we utilize near-infrared lights that are more capable of penetrating and distinguishing different materials, compared to visible lights [45]. For 3D printing, we can use filaments of two different colors (such as PLA-blue and PLA-white).

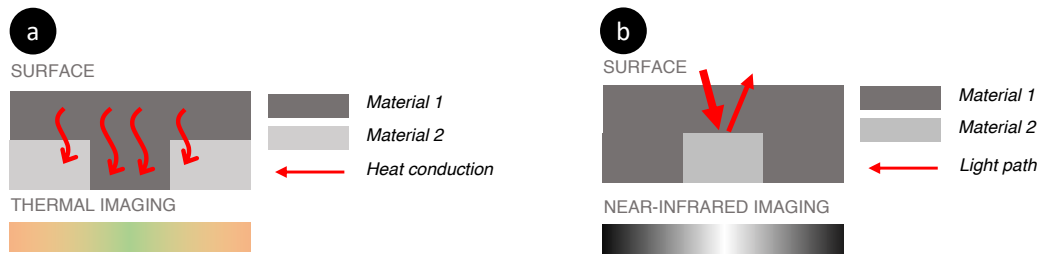


Fig. 3. Illustrations of the two reading approaches. Bottom part demonstrates the imaging patterns.

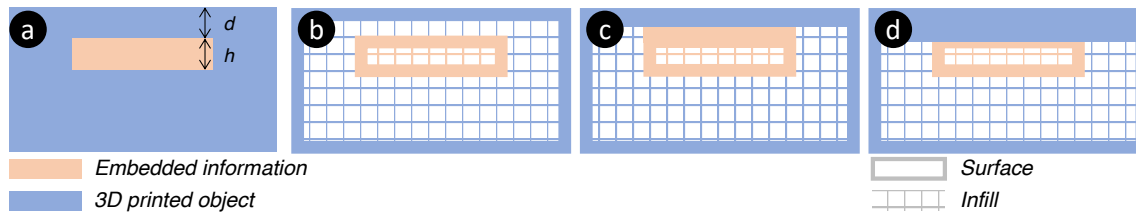


Fig. 4. Fabrication methods. (a) Illustration of the vertical cross-section. (b) Normal fabrication method. (c) The “surface-join” fabrication method. (d) The “surface-fill” fabrication method.

In this paper, we demonstrate how to read the embedded information using a thermal camera and a near-infrared scanner respectively. We use the Optris Xi 400¹ thermal camera, with wavelengths $8\ \mu\text{m} - 14\ \mu\text{m}$ (mid-far infrared). We also use the DLP NIRscan Nano [26] near-infrared scanner. For raster scanning, we mount the near-infrared scanner on an xy-plotter, controlled by a custom-built software. We also provide a supplementary video demonstrating our system with both reading devices.

3.3 Fabrication methods

We propose one fabrication technique for thermal imaging, and another for near-infrared imaging (Figure 3). Both fabrication methods use the same design models (*i.e.*, the same stl files for slicing).

- (1) *Surface-join, for thermal imaging*: As illustrated in Figure 4 (c), the “surface-join” denotes the surface layers of the object and the embedded information model are joined together. In slicing software, this is done by thickening the top or bottom layer of both the object model and the information model. This enables the thermal conduction between the object’s surface layers and the information model.
- (2) *Surface-fill, for near-infrared imaging*: As illustrated in Figure 4 (d), the “surface-fill” denotes the surface layers of the object are filled until the top of the 3D model representing the information. In slicing software, this is done by thickening the surface layer of the object model only. This is for near-infrared imaging and to prevent light scattering due to the non-uniformed infill material (filament and air) between the surface layers and the top of information model for reflection.

We note that our two methods are exclusive. Depending on specific applications and use cases, either method should be chosen for fabrication. We show various examples in the following section and provide comprehensive design guidelines in Table 3.

¹<https://www.optris.com/optris-xi-400>

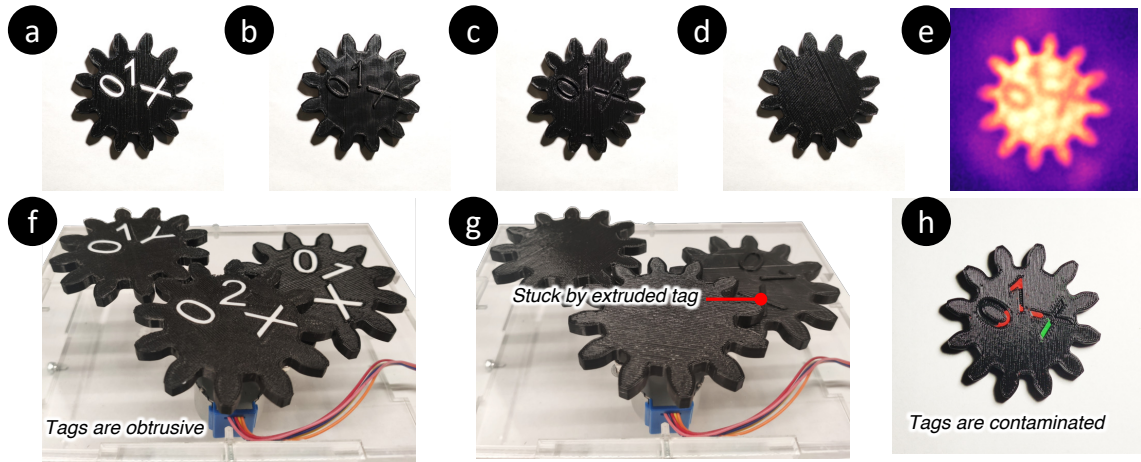


Fig. 5. Demonstration of different tagging methods by printings. The example is to 3D print a tag for a gear with the part number (01X). (a) The tag is printed on the surface using another color. (b) The tag is printed above the surface with extrusion upwards. (c) The tag is printed by extruding the tag inwards (like engraving). (d) The tag is printed under the surface. (e) The tag is read under the thermal camera for the object in (d), after the surface is warmed by hand. (f) Illustration of multiple gears with labels on the surface. (g) Illustration of malfunctioning gears tagged by extrusion in (b). (h) Illustration of visual contaminated tagged in (c).

4 EXAMPLE APPLICATIONS

InfoPrint enables various applications by embedding information inside 3D printed objects using off-the-shelf FDM 3D printers and filaments, without requiring extra procedures (such as assembly), or software modifications. We exemplify the applications including tagging 3D models, interactive thermal displays, and hand-signing (autographing) 3D prints. We present the design details in Section 6.1 below. We also demonstrate our application in the supplementary video.

4.1 Tagging 3D models

Conventional tagging methods for 3D printed objects are usually performed on the surface of the object. Such a method can alter not only the appearance of the object, but also constrains its shape or even functionality (Figure 5). In particular, for comparison, we include examples using the most common conventional tagging methods: (a) Tagging on the surface using another color. (b) Tagging by extruding outwards. (c) Tagging by extruding inwards (like engraving). Furthermore, we consider two types of tags as seen below.

Serial number: Serial numbers can be used to tag different objects with similar designs. For the examples shown in Figure 5f and g, we include three gears composed in a gearbox, tagged as “01X”, “02X” and “01Y”. The gearbox itself can be used as part of mechanical design, educational activity or exhibition. For example, in an education setting, *InfoPrint* could let students try and figure out the correct placement of the gears, whilst also embedding hidden information as hints for the students to read in case if they need help. Compared to other methods, our method is unobtrusive and does not affect the design functionality.

Binary data: Binary data can be used to store metadata for the object, e.g., the key or ID for a database entry that stores detailed information of a print or the design. For example, as shown in Figure 6, a tool can be printed using different materials (e.g., ABS or PLA) or different colors. The objects may not be easily distinguished after being printed. Since a

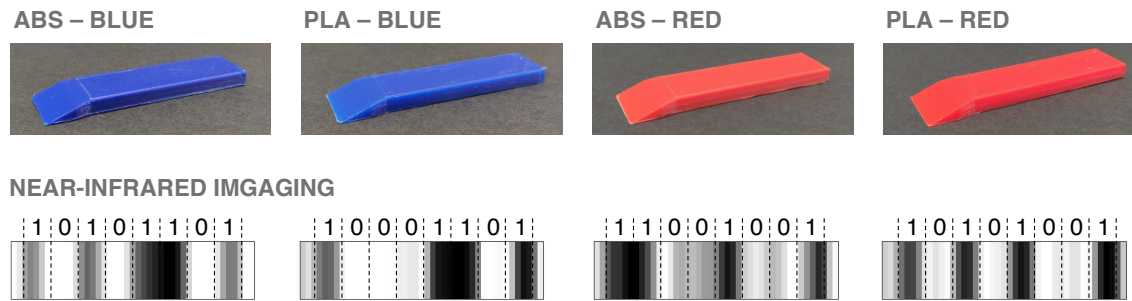


Fig. 6. Examples of tagging 3D printed tools with binary data. Embedded tags are robust for frequent and heavy use, compared to tags on the surface.

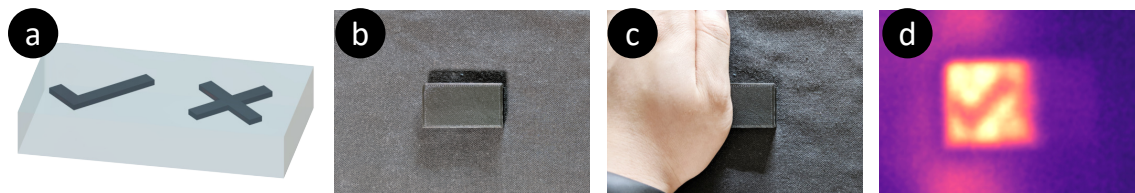


Fig. 7. Example of a 3D printed interactive thermal display. (a) The model design with different information embedded on the left part and the right part respectively. (b) The printed object with information embedded. (c) Selectively hand-warm the left part of the object. (d) The information on the left side is imaged under the thermal camera, while the information on the right side remains hidden.

tool can be frequently and heavily used, tags on the surface can be easily damaged (*e.g.*, due to scratching or abrasion). In contrast, *InfoPrint* embeds information under the surface and reduces the likelihood of damage to the tags.

4.2 Interactive thermal displays

To read the embedded information, one of the approaches we leverage is thermal conduction (Section 3.2). The information can be imaged after applying heat on the surface, *e.g.*, through warm hands. This enables a new way of interacting with a 3D printed object. As demonstrated in Figure 7, we embed two pieces of information into an object. The information can be selectively revealed by interacting with a specific part of the object (left or right), while the other part remains hidden.

Security code. In practice, such an interaction can be used for security purposes. For example, most credit cards have a CVV2 (Card Verification Value 2) code on the back side. Such a number is used for reducing credit card fraud when the card is not present for transaction [19]. However, the CVV2 code is usually printed, affording easy malicious access for potential data breaches. In similar design, the grid authentication, where the user has a grid card containing a matrix of codes for two-factor authentication is also subject to data breach risks, since the grid card codes are visible and can be photographed [5]. *InfoPrint* could address the above mentioned issues as it hides the secret information (*i.e.*, codes) under the surface. The codes can be revealed for a short period of time (detailed in Section 5.2) by interacting with the object whenever required. In addition, the location of information can be known only to the user, further improving the security of the data.

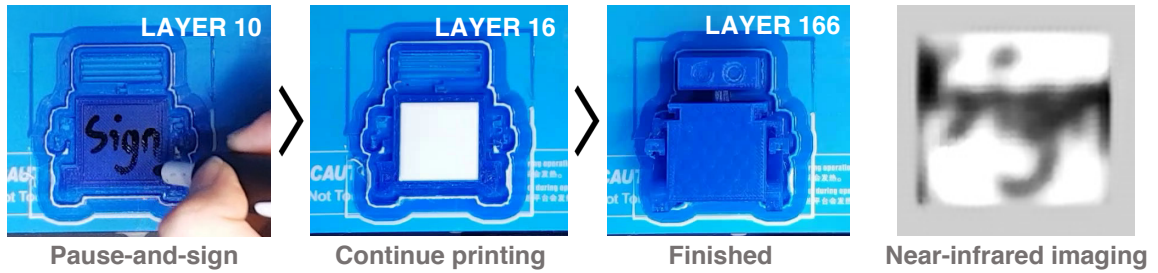


Fig. 8. Demonstration of autographing inside a 3D printed object. **Layer 10**: The autograph is signed by pausing the print job. The job is resumed after autographing. **Layer 16**: A reflective plate is printed using PLA-White. **Layer 166**: The job is finished. After printing, the autograph can be imaged by the near-infrared scanner.

Hidden tokens for social activities. *InfoPrint* can also be used in social settings such as escape rooms and board games, with temporal uncovered information. For example, objects with hidden tokens can be placed or installed in an escape room as concealed clues of puzzles. The token can only be read after interacting with the object while holding a thermal camera (e.g., recent smartphones are equipped with thermal camera such as [3], or mobile thermal cameras such as [4]). Such a design can also be used for board games, where players can be assigned with different roles using tokens or cards. With *InfoPrint*, we can create hidden tokens that can only be seen under a thermal camera after interacting with the token. For instance, a player can act as the “oracle” holds a thermal camera to identify other players’ roles. Potentially, this may provide more possibilities to design such social activities, compared to using visible or covered tokens.

4.3 Extension: autographing unique or non-fungible 3D prints

Finally, as an extension to information embedding, *InfoPrint* enables autographing inside the 3D prints. The 3D prints can then be treated as a unique object (such as an artwork), or a non-fungible object, as the autograph cannot be erased or modified (compared to autograph on the surface). As a demonstration, we show a robot model with an autograph under its back surface in Figure 8. The autograph is then imaged using the near-infrared scanner. Not only can autographs be encoded using *InfoPrint*, but other hand-written information, e.g., text, icons or binary data with precise hand-draw. In addition, the handwritten information (e.g., autograph) can be modeled and shared with the object design as a unique digital signature of the design.

5 EVALUATION AND VALIDATION

Finally, we evaluate our information embedding method to better understand its limitations, including using two different imaging approaches: thermal imaging and near-infrared imaging. A comparison between the two approaches is shown in Table 1. Furthermore, based on our results, we derive design guidelines for information embedding and reading using an FDM 3D printer for different use cases. The guidelines are included at the end of this section (Table 3).

5.1 Samples

For systematic evaluation we adopt information encoding conventions previously used in literature [33, 77], and consider a 4×4 binary matrix as the embedded information. Such a matrix can also be considered as a bitmap for non-binary data. The binary matrix is randomly generated, with 8 bits being 1s and the other 8 being 0s, with the top-left bit fixed

Table 1. Comparison between thermal (mid- to far-infrared) and near-infrared imaging methods

Imaging Method	Reading Speed	Information Density	Depth	Infill Density	Color
<i>Thermal</i> (Mid- to far-infrared)	Instant	≥ 5 mm per pixel	≤ 1 mm	$\leq 20\%$	Any color
<i>Near-infrared</i>	Tens of minutes	≥ 3 mm per pixel	≤ 3 mm	Any	Non-black (outside) + white (inside)



Fig. 9. Ground truth

as 1 as the anchor bit (Figure 9). The matrix is embedded into a cube with dimensions $W \times D \times H = 30 \times 30 \times 15$ mm. We then fabricate the cube with different print settings, including:

- (1) Information depth (d): The minimal distance between the surface and the information surface. As illustrated in Figure 4.
- (2) Information density (X): The block size (*i.e.*, the size of each bit or pixel) in the matrix, measured by *mm per pixel*.
- (3) Infill percentage: The infill percentage of the model. Both printer’s heads use the same value. We vary the infill percentage as 10%, 20%, 40% and 80%, considering the use case of modeling, standard printing tools, functional tools and heavily used tools, respectively.

For fabrication, all samples are printed using a low-cost off-the-shelf dual-head FDM 3D printer (FlashForge Creator Pro 2²). The information models (*i.e.*, the matrix) are printed using PLA-white filaments. The cube models are printed using PLA-black filaments and PLA-blue filaments, for thermal imaging and near-infrared imaging, respectively. The colors are commonly available and chosen based on our preliminary tests of performance. We also validate our results using other colors. We refer to the example applications demonstrated in Section 4 above. Other parameters are fixed for feasibility and consistency (for example, we chose honeycomb for an infill pattern, and set the information height to 1 mm. Nevertheless, we consider these parameters as negligible).

5.2 Thermal imaging

5.2.1 Reading process.

We first perform a heat transfer onto the surface of an object embedded with information. The information is revealed when the heat dissipates into the under-surface layers of the object. We record the whole process using the thermal camera and save the data as csv files, at the fastest rate specified by the thermal camera software (5 - 7 frames per second). For each frame, the following two-stage decoding pipeline is performed to decode the matrix into binary data:

- (1) *Normalization*: After reading the frame data, we first denoise the frame using a Gaussian blur filter (window size = 5×5), and normalize the values to the range between 0 and 255.
- (2) *Binarization 1*: The frame is binarized using Otsu’s method. Since the thermal imaging varies in time, we use Otsu’s method instead of a selected threshold for better robustness.
- (3) *Contour detection 1*: The contour detection algorithm is applied to the binary frame. This step is to detect the contour of the object (*i.e.*, cube).
- (4) *Cropping*: The normalized frame is cropped using the detected contour with the largest area.
- (5) *Binarization 2*: The cropped frame is binarized using Otsu’s method. Since Otsu’s method is based on the histogram of the image, this second-stage binarization can help the algorithm to better find the threshold and further increase the robustness of the decoding process.

²<https://www.flashforge.com/product-detail/51>

- (6) *Contour detection 2*: The contour detection algorithm is applied to the cropped binary frame.
- (7) *Sampling and decoding*: The center of the top-left contour is used as the anchor point for sampling. A 4×4 sampling matrix is then derived and decoded to binary data. For evaluation, the spacing between sample points is predefined.

A demonstration of thermal imaging and decoding results are shown in Figure 10 (top). We note that the steps above are only for evaluation purposes. In practice, this may not be required for human-readable non-binary information as it does not require decoding (e.g., board game token and interactive display).

5.2.2 Data collection.

We first test the imaging results at different temperature conditions. To avoid interference from other parameters, we maintain constant information depth, information density (size) and infill percentage as 1 mm, 5 mm and 10% respectively. Furthermore, considering a practical scenario, we keep the 3D printed object at room temperature ($27 \pm 2^\circ\text{C}$). We then prepare four palm-sized bags of sand (made of 100% cotton calico) at four temperature conditions: “cold” ($10 \pm 2^\circ\text{C}$), “cool” ($20 \pm 2^\circ\text{C}$), “warm” ($40 \pm 2^\circ\text{C}$) and “hot” ($50 \pm 2^\circ\text{C}$). The sand bags were heated overnight for 12 hours in a temperature-controlled warm-cool dual-mode car fridge to ensure the desired temperature was reached. The temperature errors are caused by the highly dynamic nature of heat dissipation and measurement errors of the thermal camera. Each sand bag is then placed and pressed on top of the cube for three seconds to ensure even and sufficient contact (the surface under which the matrix is embedded). The whole process is recorded by the thermal camera for 60 seconds, resulting in around 360 frames collected per condition (varies due to the thermal imaging software).

In addition to the four above-mentioned controlled conditions, we include an example for practical use – using a hand to warm-up the cube to reveal the information. Because hand temperature varies for different people at different times of the day [79], we first regulate the hand temperature using an air-activated hand-warmer. The regulated hand temperature is $35 \pm 2^\circ\text{C}$, which is within the normal human temperature range [25]. In practice, instead of using an air-activated hand-warmer, this step can be done in other ways, e.g., through hand rubbing.

5.2.3 Reading window.

For each frame, the decoding algorithm is executed to detect the binary matrix and calculate the accuracy as the number of bits correctly retrieved divided by 16. Since the thermal camera is very sensitive and requires continuous calibration while recording (performed automatically), a few frames are corrupted before or during calibration [44]. We exclude those corrupted frames by removing the outliers with performance below the 0.2 quantile. We note this phenomenon does not impact practical use of the camera as it only affects the frames imminent to the calibration.

Finally, we calculate the reading window lengths as the duration of error-free decoding (when accuracy = 1.0). The results are shown in Figure 10. As an example, we demonstrate the reading process using the hand-warming condition that is more practical than using a sandbag. Evaluation results for all conditions are included in Appendix Figure 1. We observe that under all conditions, the embedded information can be successfully read immediately after heat transfer. The maximal error-free reading window length is 12 seconds after the sandbag leaves the surface of the cube, achieved by “cold”, “cool” and “warm” conditions. The reading window lengths for “hot” and “hand” conditions are 9 seconds and 8 seconds respectively. This may be caused by the variation of heat dissipation under different conditions [7]. In particular, the heat dissipates faster with larger temperature differences³. Also, for the “hot” condition, the heat dissipates to both the ambient air and into the 3D object.

³Rate of heat flow = $-kA \cdot \Delta T / \Delta x$, where k is the thermal conductivity, A is the heat emitting area, ΔT is the temperature difference and Δx is the material thickness. In our experiments, ΔT varies.

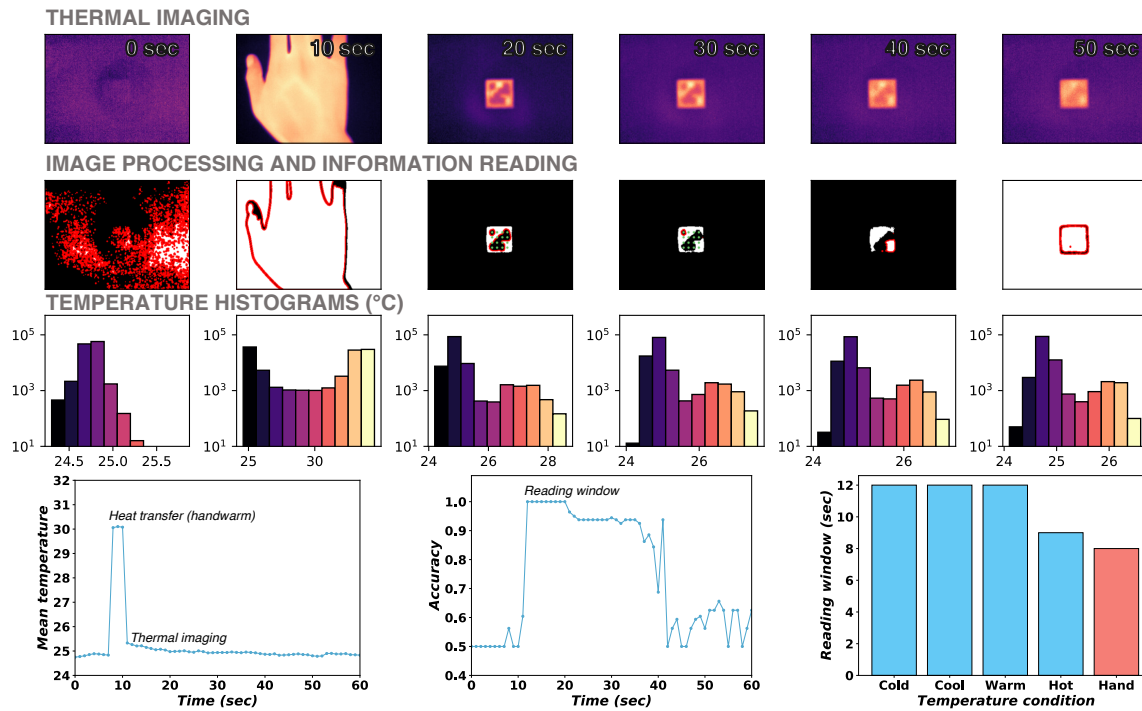


Fig. 10. Illustration thermal imaging results. The example demonstrates the hand-warming condition for thermal transfer. The colors in the histograms of different bins represent the colormap for the thermal images.

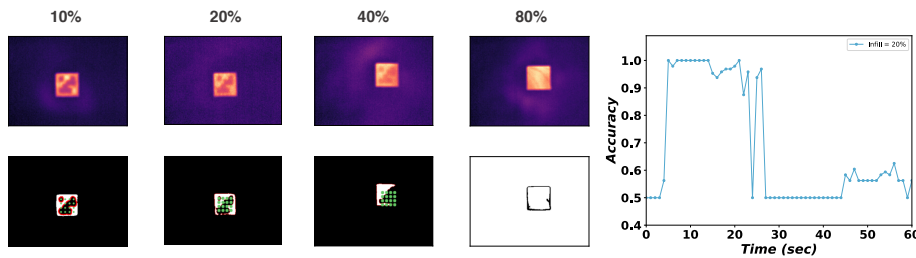


Fig. 11. Illustration of thermal imaging with different infill percentages. The figure on the right shows the accuracy in time for 20% infill percentage.

5.2.4 Other parameters.

Infill percentage. We further test the thermal imaging at different infill percentages. The initial thermal transfer is applied by hand-warming. Our reading succeeds at infill percentage of 20% and fails at 40%. The result is expected because a higher infill percentage acquires more heat. The more heat dissipates to the infill prints, the smaller the temperature difference is between the areas embedded with information model and those without, yielding more blurred thermal images. The results are shown in Figure 11.

Information density and depth. Our reading fails at higher information density or greater depth (information density $X = 4 \text{ mm per pixel}$ and depth $d = 2 \text{ mm}$). Similarly, this is limited by the principle of heat dissipation. For a higher information density, the infill prints take relatively more heat. While for the information in a greater depth, the heat dissipates through a longer path to the information model, resulting in more heat loss and less temperature differences between areas embedded with information and those without. The results are illustrated in Appendix Figure 2 and 3.

5.3 Near-infrared imaging

5.3.1 Reading process.

As briefed in Section 3, the samples are raster scanned by a near-infrared scanner mounted on an xy-plotter. For scanning, we set the raster step size as 1 mm , and home the scanner to the pre-defined area. The scanning resolution is 24×24 , resulting 576 near-infrared spectra for each image. The scanner's settings are identical to literature [29–31] ($900 \text{ nm} - 1700 \text{ nm}$ wavelength range, 228 nm wavelength resolution, 7.03 nm light pattern width, and 0.635 ms exposure time). As a result, the raw dimension for a near-infrared image is $24 \times 24 \times 228$. For each image, the following processing pipeline is performed:

- (1) *Normalization:* The mean value of each spectrum is computed across the near-infrared wavelengths as the pixel value. Then the image is normalized to the range between 0 and 255.
- (2) *Super-resolution:* We adopt a pre-trained deep-learning based super-resolution model to upsample the image by four times [14]. Since the raster-scanned resolution is low, this step can enhance the imaging quality, yielding a higher resolution of 96×96 .
- (3) *Binarization:* The image is binarized using a simple thresholding method. We empirically select 0.4 of the maximal value as the threshold for all images.
- (4) *Contour detection and decoding:* The contour detection and decoding algorithm is applied to the binary image. This step is identical to Step (6) and (7) for thermal imaging.

Similar to the thermal imaging evaluations, we calculate the decoding accuracy as the performance for each condition.

5.3.2 Information depth.

We first evaluate the reading accuracy at different information depths. The information density (block size) and infill percentage are fixed to 5 mm and 10% respectively. As clarified in Section 3, we use the surface-fill technique to fill the layers between the information model and the surface.

The results are shown in Figure 12. It can be observed that the image quality decreases as the depth increases. For decoding, we succeeded in reading the binary data until depth $d = 3 \text{ mm}$. As scarce near-infrared lights penetrate deeper and reflect back ($d > 3 \text{ mm}$), the images become too blurry to read. It is worth noting that the information is visible with depth $d = 1 \text{ mm}$. Therefore, in practice, a depth $d \geq 2 \text{ mm}$ is suggested. We show more visibility tests in Section 5.4 and provide guidelines in Table 3.

5.3.3 Information density.

Next, we test the information density by varying the block size of the information matrix. The information depth and infill percentage are fixed to $d = 2 \text{ mm}$ and 10% respectively. The results are shown in Figure 13. Our reading method can decode the data from block sizes as small as $X = 3 \text{ mm}$. Although the matrix itself can be successfully detected until $X = 1 \text{ mm}$, the decoding results are not perfect and the retrieved images are blurry.

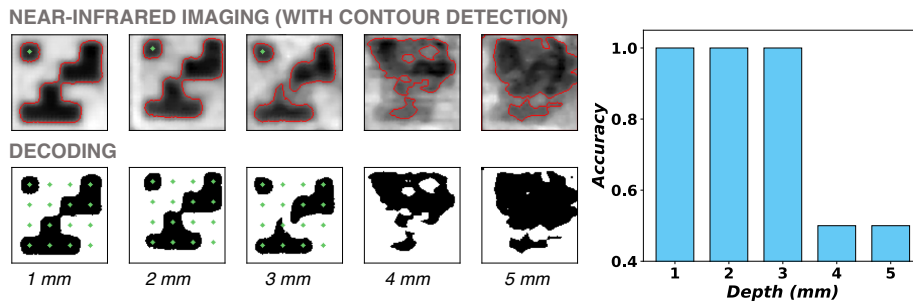


Fig. 12. Near-infrared imaging and decoding results with different information depth.

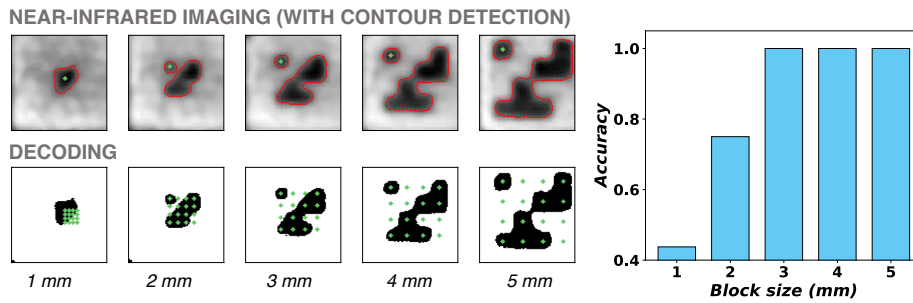


Fig. 13. Near-infrared imaging and decoding results with different block sizes (information density).

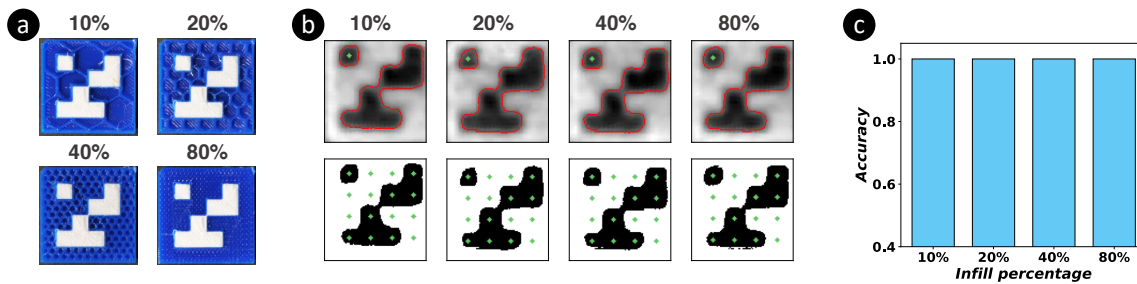


Fig. 14. Near-infrared imaging with different infill percentages. (a) Cross-section for different infill percentages. Photos are transposed for illustrations. (b) Imaging (top row) and reading (bottom row) results. (c) Reading accuracy for the samples.

5.3.4 Infill percentage.

Further, we evaluate the near-infrared imaging with different infill percentages. Aligned with the thermal imaging evaluation, we vary the infill percentages: 10%, 20%, 40% and 80%. The information depth and block size are fixed at $d = 2 \text{ mm}$ and $X = 5 \text{ mm}$ respectively. The results are shown in Figure 14. The imaging results are similar, with perfect reading results for all conditions. This result confirms that the effect of the infill parameter is negligible for near-infrared imaging, as we use the aforementioned “surface-fill” technique for fabrications.

5.3.5 Color.

In addition, we test the near-infrared imaging method using different colors. In particular, we vary the material color for

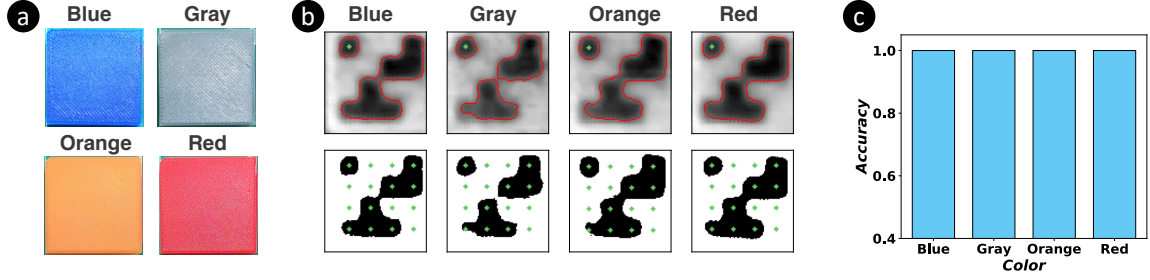


Fig. 15. Near-infrared imaging and decoding results with different colors. (a) Samples printed using different colored materials. Photos are transposed for illustrations. (b) Imaging (top row) and reading (bottom row) results. (c) Reading accuracy for the samples.

Table 2. Visibility test results for different samples.

Color	Surface-fill (near-infrared imaging)			Surface-join (thermal imaging)
	$d=1\text{ mm}$	$d=2\text{ mm}$	$d=3\text{ mm}$	
Blue	Visible	Invisible	Invisible	Unobtrusive
Red	Visible	Invisible	Invisible	Unobtrusive
Orange	Visible	Unobtrusive	Invisible	Visible
Gray	Visible	Invisible	Invisible	Visible
Black	Invisible	Invisible	Invisible	Invisible

the object (*i.e.*, the cube) while keeping the color for the information body as white. Five colors are chosen for testing: blue, gray, orange, red and black. We demonstrate the results in Figure 15. For the non-black colors, the readings are all accurate. While for the black color, we cannot extract any information inside using near-infrared light.

In principle, the black material absorbs the majority of light (both visible and infrared), and reflects very little. This characteristic makes the black material ideal for information embedding using thermal imaging, as we tested above. In contrast, the non-black materials are in fact translucent. Furthermore, near-infrared light can penetrate deeper than visible light, as we clarified in Section 3. This characteristic makes non-black colors more suitable for information embedding using the near-infrared scheme.

5.4 Visibility to the human eye

Finally, we test the visibility of information embedding using different colors, as we aim to embed information in an unobtrusive manner. For the visibility tests, the following samples are prepared, considering to be practical scenarios:

- (1) Thermal imaging samples: For thermal imaging, we fabricate the samples with information depth $d = 1\text{ mm}$, with the “surface-join” fabrication technique. The same material is used for both the information model (*i.e.*, the matrix) and the object model (*i.e.*, the cube).
- (2) Near-infrared imaging samples: For near-infrared imaging, we vary the information depth in $d = 1\text{ mm}$, 2 mm and 3 mm . The information model is printed using PLA-white, while the object model is printed using different colors.

For both thermal imaging samples and near-infrared imaging samples, we use the same color set above for the visibility test (*i.e.*, blue, gray, orange, red and black). In total, $(1\text{ thermal sample} + 3\text{ near-infrared samples}) \times 5\text{ colors} = 20\text{ samples}$ are fabricated for the visibility tests.

Table 3. Guidelines of information embedding into 3D prints

Design aspect	Design target	Design space			Examples / use cases
		Color	Depth (d)	Imaging	
Appearance	Visible	Non-black	$\leq 1 \text{ mm}$	-	Generic tagged objects with visible under-surface information
	Unobtrusive	Non-black	$1 \text{ mm} < d \leq 2 \text{ mm}$	Near-infrared	Tagged artworks, models, designs requiring aesthetics
	Invisible	Non-black	$2 \text{ mm} \leq d \leq 3 \text{ mm}$	Near-infrared	Tagged artworks, models, designs requiring aesthetics
Black		$d \leq 1 \text{ mm}$	Thermal	Tangible & invisible tokens, dynamic displays	
Functionality	Non-functional	Non-black	$d \leq 3 \text{ mm}$	Either ¹	Generic tagged objects (standard prints)
		Black	$d \leq 1 \text{ mm}$	Thermal	
	Functional	Non-black	$d \leq 3 \text{ mm}$	Near-infrared	Tagged tools, long-term use components
Information density (X , mm per pixel)	$X \geq 5$	Non-black	$d \leq 3 \text{ mm}$	Near-infrared	Objects embedded with large icons, texts or low-density data
		Black	$d \leq 1 \text{ mm}$	Thermal	
	$3 \leq X \leq 5$	Non-black	$d \leq 3 \text{ mm}$	Near-infrared	Non-fungible autographed prints, objects embedded with small icons, texts or high-density data.
Reading speed	Instant	Black	$d \leq 1 \text{ mm}$	Thermal	Board game token, dynamic display, tags requiring instant reading
	Not instant	Non-black	$d \leq 3 \text{ mm}$	Either ¹	Generic objects tagged under the surface

¹ Refer to Table 1 for more details.

We classify the visibility into “visible”, “unobtrusive” and “invisible”, aligned with the literature [11, 33]. For classification, two researchers first label the samples independently. For the controversial samples, a third researcher is included to decide the final labels independently. The ground-truth information is provided for reference. All samples are inspected in a well-illuminated office (illuminance $> 350 \text{ lx}$). The results are shown in Table 2. We run a Cohen’s kappa test to measure the inter-rater reliability. The Cohen’s kappa coefficient $\kappa = 0.76$, showed substantial agreement for the initial rating (3 out of 20 labels are controversial). For the samples printed by the “surface-fill” technique, we observe that the embedded information can be directly seen for depth $d = 1 \text{ mm}$. Whereas the embedded information is invisible for depth $d \geq 2 \text{ mm}$, except for the orange color (unobtrusive). For the “surface-join” case, only the black samples are invisible, while the blue and red samples are unobtrusive.

6 DISCUSSION

6.1 Design guidelines

We have systematically explored multiple ways of embedding information in 3D objects, and provide a thorough evaluation of multiple parameters for fabrication and reading. Given our evaluation results, we now provide design

guidelines for embedding information into 3D printed objects using an FDM 3D printer, as summarized in Table 3. We cover four design aspects for embedding information into a 3D printed object as follows:

- (1) *Appearance: Whether the embedded information can be seen directly.* For designs with appearance-related constraints, we recommend to embed information at a depth of $d \geq 2 \text{ mm}$ with colored materials (refer to the example application shown in Figure 6). Alternatively, if the design can be fabricated using a black material, the information depth should be $d \leq 1 \text{ mm}$ (refer to the example application in Figure 7).
- (2) *Functionality: Whether the printed objects are functional.* A typical functional print requires a high infill density. Since for thermal imaging the maximal infill percentage is 20%, we recommend using colored material incorporated with near-infrared imaging for embedding information into a functional printed object (refer to the example application shown in Figure 6).
- (3) *Information density: Whether the embedded information requires high density.* For information density higher than (or pixel size smaller than) 5 mm per pixel , we recommend the embedding technique with near-infrared imaging, using the “surface-fill” fabrication technique. In addition, a deep-learning based super-solution method can further increase the image quality for high-density information (refer to the example application shown in Figure 8).
- (4) *Reading speed: Whether an instant reading is required.* For embedded information that requires instant reading, we recommend embedding information incorporated with thermal imaging. Also, a thermal camera is more ubiquitous compared to a near-infrared device (e.g., a mobile thermal camera [4] or a smartphone with thermal camera [3]).

6.2 Limitations and future work

We note several limitations of *InfoPrint*, which need to be addressed in our future work and might further expand the design space and use cases.

- We only tested *InfoPrint* on an FDM printer. In principle, our method can also be applied to other 3D printing and digital fabrication techniques, such as SLA (Stereolithography) 3D printers and laser cutters that are also popular and feasible for practical use. In particular, incorporating multiple digital fabrication tools is considered a promising way to further expand the design space and accelerate design pipeline [8].
- The information density of *InfoPrint* is not very high (up to 3 mm per pixel). This limitation is mainly caused by the resolution of our imaging devices. As a complement, we utilized several computer vision algorithms to enhance the imaging quality. In the short term, the issue can be alleviated by tuning and adopting new computer vision methods that evolved rapidly in recent years [73]. In the long-term, as the hardware upgrades, the imaging quality improves, resulting in higher information density in the future.
- Also, for the evaluation, we only included the binary case in a machine-readable way. For the texts and icons, the readability may vary among users. As we focus on the embedding technique in this work, it would be beneficial to run a user-study for testing the readability for different information types.
- Our reading devices are currently not mobile. For thermal imaging, there are several mobile thermal cameras that are commercially available [4]. We also observe the emergence of smartphones integrated with a thermal camera [3]. Mobile thermal cameras and smartphones with built-in thermal cameras should be tested in future work to determine

the feasibility of *InfoPrint* in everyday scenarios. Furthermore, for near-infrared imaging, we note that the already-popular depth camera for many recent smartphones using near-infrared wavelengths [18] can potentially be used as a reading device for *InfoPrint*. Future studies can focus on developing mobile apps utilizing those smartphone components.

- For the information embedding scheme, our design is limited to a flat surface. In practice, many designs may not include a flat surface. Therefore, future work could explore a technique for embedding information under a curved surface.

7 CONCLUSION

In this paper, we presented a technique to embed information invisible to the eye inside 3D printed objects. The information can be integrated and printed with the object directly, using off-the-shelf dual-head FDM 3D printers. For retrieving the information, we adopted and evaluated two methods, thermal imaging and near-infrared imaging, respectively. Based on the evaluation results, we proposed design guidelines of embedding information for different scenarios. Applications include interactive thermal displays, hidden board game tokens, tagging functional printed objects, and autographing non-fungible fabrication work, with more use cases enabled by expanding the design space of digital fabrications with our method and future work.

REFERENCES

- [1] 2021. Autodesk Fusion 360. <https://www.autodesk.com.au/products/fusion-360> Last accessed on 2021-Aug-29.
- [2] 2021. Blender. <https://www.blender.org> Last accessed on 2021-Aug-29.
- [3] 2021. Cat phones: Rugged Phones. <https://www.catphones.com/> Last accessed on 2021-Aug-29.
- [4] 2021. Thermal Imaging | Teledyne FLIR. <https://www.flir.com.au/> Last accessed on 2021-Aug-29.
- [5] Mohammed Aamir Ali, Muhammad Ajmal Azad, Mario Parreno Centeno, Feng Hao, and Aad van Moorsel. 2019. Consumer-facing technology fraud: Economics, attack methods and potential solutions. *Future Generation Computer Systems* 100 (2019), 408–427. <https://doi.org/10.1016/j.future.2019.03.041>
- [6] Moritz Bächer, Benjamin Hepp, Fabrizio Pece, Paul G. Kry, Bernd Bickel, Bernhard Thomaszewski, and Otmar Hilliges. 2016. DefSense: Computational Design of Customized Deformable Input Devices. In *Proceedings of the 2016 CHI Conference on Human Factors in Computing Systems*. Association for Computing Machinery, New York, NY, USA, 3806–3816. <https://doi.org/10.1145/2858036.2858354>
- [7] Theodore L Bergman, Frank P Incropera, David P DeWitt, and Adrienne S Lavine. 2011. *Fundamentals of heat and mass transfer*. John Wiley & Sons.
- [8] Dustin Beyer, Serafima Gurevich, Stefanie Mueller, Hsiang-Ting Chen, and Patrick Baudisch. 2015. Platener: Low-Fidelity Fabrication of 3D Objects by Substituting 3D Print with Laser-Cut Plates. In *Proceedings of the 33rd Annual ACM Conference on Human Factors in Computing Systems*. Association for Computing Machinery, New York, NY, USA, 1799–1806. <https://doi.org/10.1145/2702123.2702225>
- [9] Perumal Varun Chadalavada, Goutham Palaniappan, Vimal Kumar Chandran, Khai Truong, and Daniel Wigdor. 2018. ID'em: Inductive Sensing for Embedding and Extracting Information in Robust Materials. *Proceedings of the ACM on Interactive, Mobile, Wearable and Ubiquitous Technologies* 2, 3 (2018), 1–28. <https://doi.org/10.1145/3264907>
- [10] Xiang 'Anthony' Chen, Stelian Coros, and Scott E. Hudson. 2018. Medley: A Library of Embeddables to Explore Rich Material Properties for 3D Printed Objects. In *Proceedings of the 2018 CHI Conference on Human Factors in Computing Systems*. Association for Computing Machinery, New York, NY, USA, 1–12. <https://doi.org/10.1145/3173574.3173736>
- [11] Arnaud Delmotte, Kenichiro Tanaka, Hiroyuki Kubo, Takuya Funatomi, and Yasuhiro Mukaigawa. 2020. Blind Watermarking for 3-D Printed Objects by Locally Modifying Layer Thickness. *IEEE Transactions on Multimedia* 22, 11 (2020), 2780–2791. <https://doi.org/10.1109/TMM.2019.2962306>
- [12] Ruta Desai, James McCann, and Stelian Coros. 2018. Assembly-Aware Design of Printable Electromechanical Devices. In *Proceedings of the 31st Annual ACM Symposium on User Interface Software and Technology (Berlin, Germany) (UIST '18)*. Association for Computing Machinery, New York, NY, USA, 457–472. <https://doi.org/10.1145/3242587.3242655>
- [13] Mustafa Doga Dogan, Faraz Faruqi, Andrew Day Churchill, Kenneth Friedman, Leon Cheng, Sriram Subramanian, and Stefanie Mueller. 2020. *G-ID: Identifying 3D Prints Using Slicing Parameters*. Association for Computing Machinery, New York, NY, USA, 1–13. <https://doi.org/10.1145/3313831.3376202>
- [14] Chao Dong, Chen Change Loy, and Xiaoou Tang. 2016. Accelerating the super-resolution convolutional neural network. In *European conference on computer vision*. Springer, 391–407. https://doi.org/10.1007/978-3-319-46475-6_25

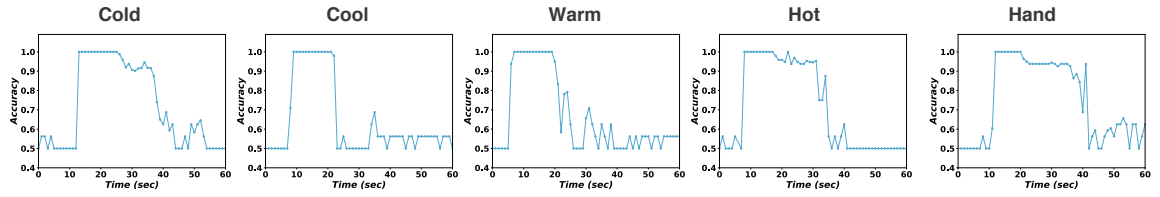
- [15] David Espalin, Danny W Muse, Eric MacDonald, and Ryan B Wicker. 2014. 3D Printing multifunctionality: structures with electronics. *The International Journal of Advanced Manufacturing Technology* 72, 5-8 (2014), 963–978. <https://doi.org/10.1007/s00170-014-5717-7>
- [16] Omid Ettehadi, Fraser Anderson, Adam Tindale, and Sowmya Somanath. 2021. Documented: Embedding Information onto and Retrieving Information from 3D Printed Objects. In *Proceedings of the 2021 CHI Conference on Human Factors in Computing Systems* (Yokohama, Japan) (CHI '21). Association for Computing Machinery, New York, NY, USA, Article 424, 11 pages. <https://doi.org/10.1145/3411764.3445551>
- [17] Jack Forman, Mustafa Doga Dogan, Hamilton Forsythe, and Hiroshi Ishii. 2020. DefeXtiles: 3D Printing Quasi-Woven Fabric via Under-Extrusion. In *Proceedings of the 33rd Annual ACM Symposium on User Interface Software and Technology* (Virtual Event, USA) (UIST '20). Association for Computing Machinery, New York, NY, USA, 1222–1233. <https://doi.org/10.1145/3379337.3415876>
- [18] Anders Grunnet-Jepsen and John N Sweetser. 2019. Intel® RealSense™ Depth Cameras for Mobile Phones. *New Technologies Group, Intel Corporation: Santa Clara, CA, USA* (2019).
- [19] Surbhi Gupta, N Malsa, and Mr Vimal Gupta. 2017. Credit Card Fraud Detection and Prevention—A Survey. *International Journal for Innovative Research in Science & Technology* 4 (2017), 1–7.
- [20] Ollie Hanton, Michael Wessely, Stefanie Mueller, Mike Fraser, and Anne Roudaut. 2020. ProtoSpray: Combining 3D Printing and Spraying to Create Interactive Displays with Arbitrary Shapes. In *Proceedings of the 2020 CHI Conference on Human Factors in Computing Systems*. Association for Computing Machinery, New York, NY, USA, 1–13. <https://doi.org/10.1145/3313831.3376543>
- [21] Chris Harrison, Robert Xiao, and Scott Hudson. 2012. Acoustic Barcodes: Passive, Durable and Inexpensive Notched Identification Tags. In *Proceedings of the 25th Annual ACM Symposium on User Interface Software and Technology* (Cambridge, Massachusetts, USA) (UIST '12). Association for Computing Machinery, New York, NY, USA, 563–568. <https://doi.org/10.1145/2380116.2380187>
- [22] Liang He, Gierad Laput, Eric Brockmeyer, and Jon E. Froehlich. 2017. SqueezePulse: Adding Interactive Input to Fabricated Objects Using Corrugated Tubes and Air Pulses. In *Proceedings of the Eleventh International Conference on Tangible, Embedded, and Embodied Interaction* (Yokohama, Japan) (TEI '17). Association for Computing Machinery, New York, NY, USA, 341–350. <https://doi.org/10.1145/3024969.3024976>
- [23] Freddie Hong, Connor Myant, and David E Boyle. 2021. Thermoformed Circuit Boards: Fabrication of Highly Conductive Freeform 3D Printed Circuit Boards with Heat Bending. In *Proceedings of the 2021 CHI Conference on Human Factors in Computing Systems* (Yokohama, Japan) (CHI '21). Association for Computing Machinery, New York, NY, USA, Article 669, 10 pages. <https://doi.org/10.1145/3411764.3445469>
- [24] Jonathan Hook, Thomas Nappay, Steve Hodges, Peter Wright, and Patrick Olivier. 2014. Making 3D Printed Objects Interactive Using Wireless Accelerometers. In *CHI '14 Extended Abstracts on Human Factors in Computing Systems* (Toronto, Ontario, Canada) (CHI EA '14). Association for Computing Machinery, New York, NY, USA, 1435–1440. <https://doi.org/10.1145/2559206.2581137>
- [25] James S Hutchison, Roxanne E Ward, Jacques Lacroix, Paul C Hébert, Marcia A Barnes, Desmond J Bohn, Peter B Dirks, Steve Doucette, Dean Fergusson, Ronald Gottesman, et al. 2008. Hypothermia therapy after traumatic brain injury in children. *New England Journal of Medicine* 358, 23 (2008), 2447–2456. <https://doi.org/10.1056/NEJMoa0706930>
- [26] Texas Instruments Incorporated. n.d. DLP NIRscan Nano Evaluation Module. <http://www.ti.com/tool/DLPNIRNANOEVLM>. (Accessed on 07/11/2018).
- [27] Yoshio Ishiguro and Ivan Poupyrev. 2014. 3D Printed Interactive Speakers. In *Proceedings of the SIGCHI Conference on Human Factors in Computing Systems* (Toronto, Ontario, Canada) (CHI '14). Association for Computing Machinery, New York, NY, USA, 1733–1742. <https://doi.org/10.1145/2556288.2557046>
- [28] Vikram Iyer, Justin Chan, Ian Culhane, Jennifer Mankoff, and Shyamnath Gollakota. 2018. Wireless Analytics for 3D Printed Objects. In *Proceedings of the 31st Annual ACM Symposium on User Interface Software and Technology* (Berlin, Germany) (UIST '18). Association for Computing Machinery, New York, NY, USA, 141–152. <https://doi.org/10.1145/3242587.3242639>
- [29] Weiwei Jiang, Gabriele Marini, Niels van Berkel, Zhanna Sarsenbayeva, Zheyu Tan, Chu Luo, Xin He, Tilman Dinger, Jorge Goncalves, Yoshihiro Kawahara, and Vassilis Kostakos. 2019. Probing Sucrose Contents in Everyday Drinks Using Miniaturized Near-Infrared Spectroscopy Scanners. *Proc. ACM Interact. Mob. Wearable Ubiquitous Technol.* 3, 4, Article 136 (Dec. 2019), 25 pages. <https://doi.org/10.1145/3369834>
- [30] Weiwei Jiang, Zhanna Sarsenbayeva, Niels van Berkel, Chaofan Wang, Difeng Yu, Jing Wei, Jorge Goncalves, and Vassilis Kostakos. 2021. User Trust in Assisted Decision-Making Using Miniaturized Near-Infrared Spectroscopy. In *Proceedings of the 2021 CHI conference on human factors in computing systems*. Association for Computing Machinery, New York, NY, USA, 1–16. <https://doi.org/10.1145/3411764.3445710>
- [31] Simon Klakegg, Jorge Goncalves, Chu Luo, Aku Visuri, Alexey Popov, Niels van Berkel, Zhanna Sarsenbayeva, Vassilis Kostakos, Simo Hosio, Scott Savage, et al. 2018. Assisted Medication Management in Elderly Care Using Miniaturised Near-Infrared Spectroscopy. *Proceedings of the ACM on Interactive, Mobile, Wearable and Ubiquitous Technologies* 2, 2 (2018), 69. <https://doi.org/10.1145/3214272>
- [32] Donghyeon Ko, Jee Bin Yim, Yujin Lee, Jaehoon Pyun, and Woohun Lee. 2021. Designing Metamaterial Cells to Enrich Thermoforming 3D Printed Object for Post-Print Modification. In *Proceedings of the 2021 CHI Conference on Human Factors in Computing Systems* (Yokohama, Japan) (CHI '21). Association for Computing Machinery, New York, NY, USA, Article 671, 12 pages. <https://doi.org/10.1145/3411764.3445229>
- [33] Dingzeyu Li, Avinash S Nair, Shree K Nayar, and Changxi Zheng. 2017. Aircode: Unobtrusive physical tags for digital fabrication. In *Proceedings of the 30th annual ACM symposium on user interface software and technology*. 449–460. <https://doi.org/10.1145/3126594.3126635>
- [34] Hanchuan Li, Eric Brockmeyer, Elizabeth J Carter, Josh Fromm, Scott E Hudson, Shwetak N Patel, and Alanson Sample. 2016. Paperid: A technique for drawing functional battery-free wireless interfaces on paper. In *Proceedings of the 2016 CHI Conference on Human Factors in Computing Systems*. 5885–5896. <https://doi.org/10.1145/2858036.2858249>
- [35] Eric MacDonald and Ryan Wicker. 2016. Multiprocess 3D printing for increasing component functionality. *Science* 353, 6307 (2016). <https://doi.org/10.1126/science.aaf2093> arXiv:<https://science.sciencemag.org/content/353/6307/aaf2093.full.pdf>

- [36] Henrique Teles Maia, Dingzeyu Li, Yuan Yang, and Changxi Zheng. 2019. LayerCode: Optical Barcodes for 3D Printed Shapes. *ACM Trans. Graph.* 38, 4, Article 112 (July 2019), 14 pages. <https://doi.org/10.1145/3306346.3322960>
- [37] Karola Marky, Martin Schmitz, Verena Zimmermann, Martin Herbers, Kai Kunze, and Max Mühlhäuser. 2020. 3D-Auth: Two-Factor Authentication with Personalized 3D-Printed Items. In *Proceedings of the 2020 CHI Conference on Human Factors in Computing Systems*. Association for Computing Machinery, New York, NY, USA, 1–12. <https://doi.org/10.1145/3313831.3376189>
- [38] Stefanie Mueller, Tobias Mohr, Kerstin Guenther, Johannes Frohnhofen, and Patrick Baudisch. 2014. FaBrickation: Fast 3D Printing of Functional Objects by Integrating Construction Kit Building Blocks. In *Proceedings of the SIGCHI Conference on Human Factors in Computing Systems (Toronto, Ontario, Canada) (CHI '14)*. Association for Computing Machinery, New York, NY, USA, 3827–3834. <https://doi.org/10.1145/2556288.2557005>
- [39] Sachith Muthukumarana, Moritz Alexander Messerschmidt, Denys J.C. Matthies, Jürgen Steimle, Philipp M. Scholl, and Suranga Nanayakkara. 2021. ClothTiles: A Prototyping Platform to Fabricate Customized Actuators on Clothing Using 3D Printing and Shape-Memory Alloys. In *Proceedings of the 2021 CHI Conference on Human Factors in Computing Systems (Yokohama, Japan) (CHI '21)*. Association for Computing Machinery, New York, NY, USA, Article 510, 12 pages. <https://doi.org/10.1145/3411764.3445613>
- [40] Marla Narazani, Chloe Egtebas, Gudrun Klinker, Sarah L. Jenney, Michael Mühlhaus, and Frank Petzold. 2019. Extending AR Interaction through 3D Printed Tangible Interfaces in an Urban Planning Context. In *The Adjunct Publication of the 32nd Annual ACM Symposium on User Interface Software and Technology (New Orleans, LA, USA) (UIST '19)*. Association for Computing Machinery, New York, NY, USA, 116–118. <https://doi.org/10.1145/3332167.3356891>
- [41] Hyunjoon Oh, Tung D. Ta, Ryo Suzuki, Mark D. Gross, Yoshihiro Kawahara, and Lining Yao. 2018. PEP (3D Printed Electronic Papercrafts): An Integrated Approach for 3D Sculpting Paper-Based Electronic Devices. Association for Computing Machinery, New York, NY, USA, 1–12. <https://doi.org/10.1145/3173574.3174015>
- [42] Simon Olberding, Sergio Soto Ortega, Klaus Hildebrandt, and Jürgen Steimle. 2015. Foldio: Digital Fabrication of Interactive and Shape-Changing Objects With Foldable Printed Electronics. In *Proceedings of the 28th Annual ACM Symposium on User Interface Software and Technology (Charlotte, NC, USA) (UIST '15)*. Association for Computing Machinery, New York, NY, USA, 223–232. <https://doi.org/10.1145/2807442.2807494>
- [43] Huaihu Peng, Jennifer Mankoff, Scott E. Hudson, and James McCann. 2015. A Layered Fabric 3D Printer for Soft Interactive Objects. In *Proceedings of the 33rd Annual ACM Conference on Human Factors in Computing Systems*. Association for Computing Machinery, New York, NY, USA, 1789–1798. <https://doi.org/10.1145/2702123.2702327>
- [44] Surya Prakash, Pei Yean Lee, Terry Caelli, and Tim Raupach. 2006. Robust thermal camera calibration and 3D mapping of object surface temperatures. In *Thermosense XXVIII*, Vol. 6205. International Society for Optics and Photonics, 62050J. <https://doi.org/10.1117/12.668459>
- [45] Gabriele Reich. 2005. Near-infrared spectroscopy and imaging: Basic principles and pharmaceutical applications. *Advanced Drug Delivery Reviews* 57, 8 (2005), 1109–1143. <https://doi.org/10.1016/j.addr.2005.01.020> Non-Invasive Spectroscopic and Imaging Techniques in Drug Delivery.
- [46] Michael L. Rivera and Scott E. Hudson. 2019. Desktop Electrospinning: A Single Extruder 3D Printer for Producing Rigid Plastic and Electrospun Textiles. In *Proceedings of the 2019 CHI Conference on Human Factors in Computing Systems*. Association for Computing Machinery, New York, NY, USA, 1–12. <https://doi.org/10.1145/3290605.3300434>
- [47] Michael L. Rivera, Melissa Moukperian, Daniel Ashbrook, Jennifer Mankoff, and Scott E. Hudson. 2017. *Stretching the Bounds of 3D Printing with Embedded Textiles*. Association for Computing Machinery, New York, NY, USA, 497–508. <https://doi.org/10.1145/3025453.3025460>
- [48] Valkyrie Savage, Colin Chang, and Björn Hartmann. 2013. Sauron: Embedded Single-Camera Sensing of Printed Physical User Interfaces. In *Proceedings of the 26th Annual ACM Symposium on User Interface Software and Technology (St. Andrews, Scotland, United Kingdom) (UIST '13)*. Association for Computing Machinery, New York, NY, USA, 447–456. <https://doi.org/10.1145/2501988.2501992>
- [49] Valkyrie Savage, Andrew Head, Björn Hartmann, Dan B. Goldman, Gautham Mysore, and Wilmot Li. 2015. Lamello: Passive Acoustic Sensing for Tangible Input Components. In *Proceedings of the 33rd Annual ACM Conference on Human Factors in Computing Systems*. Association for Computing Machinery, New York, NY, USA, 1277–1280. <https://doi.org/10.1145/2702123.2702207>
- [50] Valkyrie Savage, Ryan Schmidt, Tovi Grossman, George Fitzmaurice, and Björn Hartmann. 2014. A Series of Tubes: Adding Interactivity to 3D Prints Using Internal Pipes. In *Proceedings of the 27th Annual ACM Symposium on User Interface Software and Technology (Honolulu, Hawaii, USA) (UIST '14)*. Association for Computing Machinery, New York, NY, USA, 3–12. <https://doi.org/10.1145/2642918.2647374>
- [51] Martin Schmitz, Martin Herbers, Niloofar Dezfuli, Sebastian Günther, and Max Mühlhäuser. 2018. Off-Line Sensing: Memorizing Interactions in Passive 3D-Printed Objects. In *Proceedings of the 2018 CHI Conference on Human Factors in Computing Systems*. Association for Computing Machinery, New York, NY, USA, 1–8. <https://doi.org/10.1145/3173574.3173756>
- [52] Martin Schmitz, Mohammadreza Khalilbeigi, Matthias Balwierz, Roman Lissermann, Max Mühlhäuser, and Jürgen Steimle. 2015. Capricate: A Fabrication Pipeline to Design and 3D Print Capacitive Touch Sensors for Interactive Objects. In *Proceedings of the 28th Annual ACM Symposium on User Interface Software and Technology (Charlotte, NC, USA) (UIST '15)*. Association for Computing Machinery, New York, NY, USA, 253–258. <https://doi.org/10.1145/2807442.2807503>
- [53] Martin Schmitz, Andreas Leister, Niloofar Dezfuli, Jan Riemann, Florian Müller, and Max Mühlhäuser. 2016. Liquido: Embedding Liquids into 3D Printed Objects to Sense Tilting and Motion. In *Proceedings of the 2016 CHI Conference Extended Abstracts on Human Factors in Computing Systems (San Jose, California, USA) (CHI EA '16)*. Association for Computing Machinery, New York, NY, USA, 2688–2696. <https://doi.org/10.1145/2851581.2892275>
- [54] Martin Schmitz, Florian Müller, Max Mühlhäuser, Jan Riemann, and Huy Viet Viet Le. 2021. Itsy-Bits: Fabrication and Recognition of 3D-Printed Tangibles with Small Footprints on Capacitive Touchscreens. In *Proceedings of the 2021 CHI Conference on Human Factors in Computing Systems (Yokohama, Japan) (CHI '21)*. Association for Computing Machinery, New York, NY, USA, Article 419, 12 pages. <https://doi.org/10.1145/3411764>

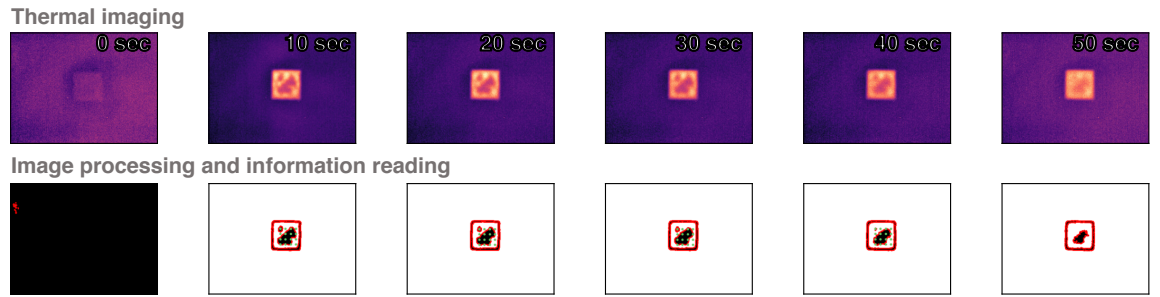
- 3445502
- [55] Martin Schmitz, Jan Riemann, Florian Müller, Steffen Kreis, and Max Mühlhäuser. 2021. Oh, Snap! A Fabrication Pipeline to Magnetically Connect Conventional and 3D-Printed Electronics. In *Proceedings of the 2021 CHI Conference on Human Factors in Computing Systems* (Yokohama, Japan) (CHI '21). Association for Computing Machinery, New York, NY, USA, Article 420, 11 pages. <https://doi.org/10.1145/3411764.3445641>
- [56] Martin Schmitz, Jürgen Steimle, Jochen Huber, Niloofar Dezfuli, and Max Mühlhäuser. 2017. Flexibles: Deformation-Aware 3D-Printed Tangibles for Capacitive Touchscreens. In *Proceedings of the 2017 CHI Conference on Human Factors in Computing Systems*. Association for Computing Machinery, New York, NY, USA, 1001–1014. <https://doi.org/10.1145/3025453.3025663>
- [57] Martin Schmitz, Martin Stitz, Florian Müller, Markus Funk, and Max Mühlhäuser. 2019. Trilaterate: A Fabrication Pipeline to Design and 3D Print Hover-, Touch-, and Force-Sensitive Objects. In *Proceedings of the 2019 CHI Conference on Human Factors in Computing Systems*. Association for Computing Machinery, New York, NY, USA, 1–13. <https://doi.org/10.1145/3290605.3300684>
- [58] Rita Shewbridge, Amy Hurst, and Shaun K. Kane. 2014. Everyday Making: Identifying Future Uses for 3D Printing in the Home. In *Proceedings of the 2014 Conference on Designing Interactive Systems* (Vancouver, BC, Canada) (DIS '14). Association for Computing Machinery, New York, NY, USA, 815–824. <https://doi.org/10.1145/2598510.2598544>
- [59] Piyarat Silapasuphakornwong, Chaiwuth Sithiwichankit, and Kazutake Uehira. 2018. Information Embedding in 3D Printed Objects Using Metal-Infused PLA and Reading with Thermography. In *NIP & Digital Fabrication Conference*, Vol. 2018. Society for Imaging Science and Technology, 202–207.
- [60] Piyarat Silapasuphakornwong, Masahiro Suzuki, Hiroshi Unno, Hideyuki Torii, Kazutake Uehira, and Youichi Takashima. 2016. Nondestructive Readout of Copyright Information Embedded in Objects Fabricated with 3-D Printers. In *Digital-Forensics and Watermarking*, Yun-Qing Shi, Hyoung Joong Kim, Fernando Pérez-González, and Isao Echizen (Eds.). Springer International Publishing, Cham, 232–238.
- [61] Piyarat Silapasuphakornwong, Hideyuki Torii, Masahiro Suzuki, and Kazutake Uehira. 2019. 3D Printing Technique That Can Record Information Inside An Object As Rewritable. In *NIP & Digital Fabrication Conference*, Vol. 2019. Society for Imaging Science and Technology, 158–161.
- [62] P Silapasuphakornwong, H Torii, K Uehira, and M Suzuki. 2019. Technique for embedding information in objects produced with 3D printer using near infrared fluorescent dye. In *Int. Conference on Advances in Multimedia*. 55–58.
- [63] Andrew Spielberg, Alanson Sample, Scott E. Hudson, Jennifer Mankoff, and James McCann. 2016. RapID: A Framework for Fabricating Low-Latency Interactive Objects with RFID Tags. In *Proceedings of the 2016 CHI Conference on Human Factors in Computing Systems*. Association for Computing Machinery, New York, NY, USA, 5897–5908.
- [64] Lingyun Sun, Yue Yang, Yu Chen, Jiayi Li, Danli Luo, Haolin Liu, Lining Yao, Ye Tao, and Guanyun Wang. 2021. ShrinCage: 4D Printing Accessories That Self-Adapt. In *Proceedings of the 2021 CHI Conference on Human Factors in Computing Systems* (Yokohama, Japan) (CHI '21). Association for Computing Machinery, New York, NY, USA, Article 433, 12 pages. <https://doi.org/10.1145/3411764.3445220>
- [65] Masahiro Suzuki, Tomohisa Matumoto, Youichi Takashima, Hideyuki Torii, and Kazutake Uehira. 2017. Information Hiding Inside 3-D Printed Objects by Forming High Reflectance Projections (ICVIP 2017). Association for Computing Machinery, New York, NY, USA, 146–150. <https://doi.org/10.1145/3177404.3177455>
- [66] Saiganesh Swaminathan, Kadri Bugra Ozutemiz, Carmel Majidi, and Scott E. Hudson. 2019. FiberWire: Embedding Electronic Function into 3D Printed Mechanically Strong, Lightweight Carbon Fiber Composite Objects. In *Proceedings of the 2019 CHI Conference on Human Factors in Computing Systems*. Association for Computing Machinery, New York, NY, USA, 1–11. <https://doi.org/10.1145/3290605.3300797>
- [67] Haruki Takahashi and Jeeun Kim. 2019. 3D Printed Fabric: Techniques for Design and 3D Weaving Programmable Textiles. In *Proceedings of the 32nd Annual ACM Symposium on User Interface Software and Technology* (New Orleans, LA, USA) (UIST '19). Association for Computing Machinery, New York, NY, USA, 43–51. <https://doi.org/10.1145/3332165.3347896>
- [68] Carlos E. Tejada, Raf Ramakers, Sebastian Boring, and Daniel Ashbrook. 2020. AirTouch: 3D-Printed Touch-Sensitive Objects Using Pneumatic Sensing. In *Proceedings of the 2020 CHI Conference on Human Factors in Computing Systems*. Association for Computing Machinery, New York, NY, USA, 1–10. <https://doi.org/10.1145/3313831.3376136>
- [69] Yutaka Tokuda, Deepak Ranjan Sahoo, Matt Jones, Sriram Subramanian, and Anusha Withana. 2021. Flowcuits: Crafting Tangible and Interactive Electrical Components with Liquid Metal Circuits. In *Proceedings of the Fifteenth International Conference on Tangible, Embedded, and Embodied Interaction* (Salzburg, Austria) (TEI '21). Association for Computing Machinery, New York, NY, USA, Article 35, 11 pages. <https://doi.org/10.1145/3430524.3440654>
- [70] Alexander D Valentine, Travis A Busbee, John William Boley, Jordan R Raney, Alex Chortos, Arda Kotikian, John Daniel Berrigan, Michael F Durstock, and Jennifer A Lewis. 2017. Hybrid 3D printing of soft electronics. *advanced Materials* 29, 40 (2017), 1703817.
- [71] Tom Valkeneers, Danny Leen, Daniel Ashbrook, and Raf Ramakers. 2019. StackMold: Rapid Prototyping of Functional Multi-Material Objects with Selective Levels of Surface Details. In *Proceedings of the 32nd Annual ACM Symposium on User Interface Software and Technology* (New Orleans, LA, USA) (UIST '19). Association for Computing Machinery, New York, NY, USA, 687–699. <https://doi.org/10.1145/3332165.3347915>
- [72] Marynel Vázquez, Eric Brockmeyer, Ruta Desai, Chris Harrison, and Scott E. Hudson. 2015. 3D Printing Pneumatic Device Controls with Variable Activation Force Capabilities. In *Proceedings of the 33rd Annual ACM Conference on Human Factors in Computing Systems*. Association for Computing Machinery, New York, NY, USA, 1295–1304. <https://doi.org/10.1145/2702123.2702569>
- [73] Athanasios Voulodimos, Nikolaos Doulamis, Anastasios Doulamis, and Eftychios Protopapadakis. 2018. Deep learning for computer vision: A brief review. *Computational intelligence and neuroscience* 2018 (2018). <https://doi.org/10.1155/2018/7068349>

- [74] Ludwig Wilhelm Wall, Alec Jacobson, Daniel Vogel, and Oliver Schneider. 2021. Scrappy: Using Scrap Material as Infill to Make Fabrication More Sustainable. In *Proceedings of the 2021 CHI Conference on Human Factors in Computing Systems* (Yokohama, Japan) (*CHI '21*). Association for Computing Machinery, New York, NY, USA, Article 665, 12 pages. <https://doi.org/10.1145/3411764.3445187>
- [75] Guanyun Wang, Fang Qin, Haolin Liu, Ye Tao, Yang Zhang, Yongjie Jessica Zhang, and Lining Yao. 2020. MorphingCircuit: An Integrated Design, Simulation, and Fabrication Workflow for Self-Morphing Electronics. *Proc. ACM Interact. Mob. Wearable Ubiquitous Technol.* 4, 4, Article 157 (Dec. 2020), 26 pages. <https://doi.org/10.1145/3432232>
- [76] Karl Willis, Eric Brockmeyer, Scott Hudson, and Ivan Poupyrev. 2012. Printed Optics: 3D Printing of Embedded Optical Elements for Interactive Devices. In *Proceedings of the 25th Annual ACM Symposium on User Interface Software and Technology* (Cambridge, Massachusetts, USA) (*UIST '12*). Association for Computing Machinery, New York, NY, USA, 589–598. <https://doi.org/10.1145/2380116.2380190>
- [77] Karl DD Willis and Andrew D Wilson. 2013. InfraStructs: fabricating information inside physical objects for imaging in the terahertz region. *ACM Transactions on Graphics (TOG)* 32, 4 (2013), 1–10. <https://doi.org/10.1145/2461912.2461936>
- [78] Junichi Yamaoka, Mustafa Doga Dogan, Katarina Bulovic, Kazuya Saito, Yoshihiro Kawahara, Yasuaki Takehi, and Stefanie Mueller. 2019. FoldTronics: Creating 3D Objects with Integrated Electronics Using Foldable Honeycomb Structures. In *Proceedings of the 2019 CHI Conference on Human Factors in Computing Systems*. Association for Computing Machinery, New York, NY, USA, 1–14. <https://doi.org/10.1145/3290605.3300858>
- [79] Alla Zontak, Samuel Sideman, Oleg Verbitsky, and Rafael Beyar. 1998. Dynamic thermography: analysis of hand temperature during exercise. *Annals of biomedical engineering* 26, 6 (1998), 988–993. <https://doi.org/10.1114/1.33>

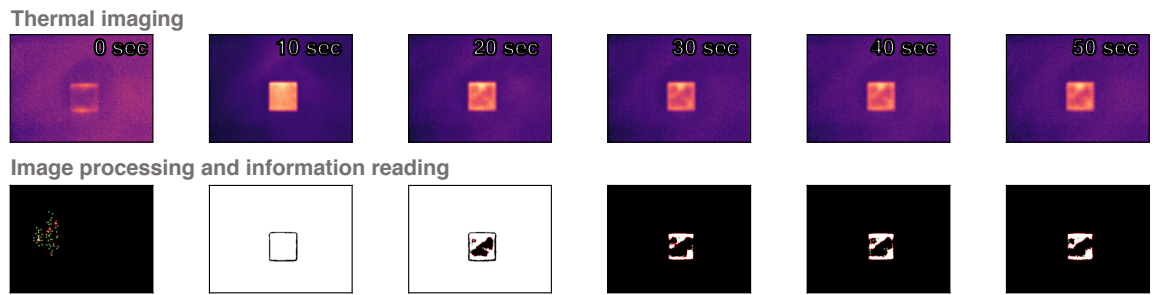
APPENDIX



Appendix Fig. 1. Thermal imaging evaluation results in different thermal transfer conditions.



Appendix Fig. 2. Illustration of thermal imaging results for information density = 4 mm.



Appendix Fig. 3. Illustration of thermal imaging results for information depth = 2 mm.